Research Square

Preprints are preliminary reports that have not undergone peer review.
They should not be considered conclusive, used to inform clinical practice,
or referenced by the media as validated information.

Aging reshapes post-traumatic immune trajectories: selective human recovery associations and complementary NAD⁺-sensitive endothelial responses

Shuaipeng Gu
Tongji Hospital, Tongji Medical College, Huazhong University of Science and Technology
Peidong Zhang
Tongji Hospital, Tongji Medical College, Huazhong University of Science and Technology
Jialiu Luo
Tongji Hospital, Tongji Medical College, Huazhong University of Science and Technology
Shunyao Chen
Tongji Hospital, Tongji Medical College, Huazhong University of Science and Technology
Zhiqiang Lin
Tongji Hospital, Tongji Medical College, Huazhong University of Science and Technology
Yuhao Wu
Tongji Hospital, Tongji Medical College, Huazhong University of Science and Technology
Zhaohui Tang
Tongji Hospital, Tongji Medical College, Huazhong University of Science and Technology
Cong Zhang
tjzhangc@hust.edu.cn
Tongji Hospital, Tongji Medical College, Huazhong University of Science and Technology

Research Article

Keywords: Aging, Immunosenescence, Polytrauma, Immune trajectories, Endothelial remodeling, NAD⁺ homeostasis

Posted Date: November 9th, 2026

DOI: https://doi.org/10.21203/rs.3.rs-11400285/v1

License: This work is licensed under a Creative Commons Attribution 4.0 International License.
Read Full License

Additional Declarations: No competing interests reported.

Aging reshapes post-traumatic immune trajectories: selective human recovery associations and complementary NAD^+-sensitive endothelial responses

Shuaipeng Gu[1] , Peidong Zhang[1] ,Jialiu Luo[1], Shunyao Chen[1], Zhiqiang Lin[1], Yuhao Wu[1], Zhaohui Tang[1], Cong Zhang[1#]

[1] Department of Trauma Surgery, Emergency Surgery and Surgical Critical Care, Tongji Trauma Center, Tongji Hospital, Tongji Medical College, Huazhong University of Science and Technology, Wuhan 430030, China;

gusp@hust.edu.cn (S.G.); peidongzhang@hust.edu.cn (P.Z.);luojialiu@hust.edu.cn(J.L.); tjchensy@hust.edu.cn (S.C.); linzhiqiang@hust.edu.cn (Z.L.); wuyuhao@hust.edu.cn(Y.W.);tangzh@tjh.tjmu.edu.cn (Z.T.); tjzhangc@hust.edu.cn (C.Z.)

[#] Correspondence: tjzhangc@hust.edu.cn (C.Z.)

Abstract

Background: Aging affects immunity after severe injury, but its effects on the timing of post-traumatic immune remodeling and subsequent recovery remain unclear. We examined age-associated trajectories and NAD^+-sensitive endothelial remodeling as complementary evidence.

Methods: We analyzed public mouse polytrauma, longitudinal human trauma, clinical recovery, brain endothelial aging, and published NAD^+ perturbation datasets. Fixed immune programmes, a mouse-derived signature frozen before human testing, strict ortholog mapping, outcome-linked survival models, and sensitivity analyses were applied without pooling datasets.

Results: In 36 young and aged mice, immune programme differences peaked at day 1, whereas aged animals remained farther from age-matched transcriptomic baseline at day 3. A 311-gene late-response signature comprised 188 old-excess and 123 old-deficit genes. Neither component distinguished fast from slow human recovery at day 3 after correction, but day-7 old-excess scores were associated with slower subsequent recovery (hazard ratio 0.605, 95% confidence interval 0.469–0.780; adjusted q = 0.0010). Independent brain endothelial analyses revealed heterogeneous redox and barrier-associated transcription. In a published HUVEC model, NAMPT inhibition reduced endothelial transition projection to approximately 0.53, whereas nicotinamide mononucleotide restored it to approximately 1.05. Twenty-one Hallmark pathways met blockade–rescue criteria; only oxidative phosphorylation met strict cross-context criteria in a separate hippocampal model.

Conclusions: Aging was associated with a distinct late post-traumatic immune state showing selective, time-dependent links to human recovery. NAD^+-sensitive endothelial remodeling provides independent mechanistic context, not evidence of causation in trauma recovery.

Keywords: Aging; Immunosenescence; Polytrauma; Immune trajectories; Endothelial remodeling; NAD^+ homeostasis

1. Introduction

Severe injury evokes rapidly changing immune states, yet recovery is often described as the disappearance of acute inflammation. Contemporary critical-care analyses instead indicate that post-injury biology evolves along multidimensional and temporally coordinated trajectories[1]. In patients with trauma, single-cell profiling has associated faster recovery with a subacute monocyte-network transition rather than simple restoration of a healthy baseline[2]. These observations raise a geroscience question: does aging chiefly increase the early response to injury, or impair the capacity to exit that response and enter maintenance and repair states?

Aging disrupts proteostasis, mitochondrial regulation, intercellular communication and immune adaptation[3]. The response to surgical injury also varies with age and differs in important respects from accidental trauma[4]. Thus, a stronger inflammatory score is not, on its own, evidence of poorer recovery. Here, recovery competence denotes the observed capacity to coordinate transitions from injury-engaged transcriptional programmes toward maintenance and repair; it is neither a validated clinical score nor an assumption that transcriptional normalization is necessary for recovery.

Circulating and vascular compartments provide a plausible setting in which aging and injury responses intersect. Trauma-associated small extracellular vesicles (sEVs) can transfer inflammatory signals to endothelium[5]. Extracranial injury can coincide with region-specific brain inflammatory transcription[6]. Vascular populations are heterogeneous[7]. Age-related changes in endothelial transport are not always captured by RNA measurements[8]. Circulatory cues can influence the aging brain in a context-dependent fashion[9, 10]. Accordingly, HUVEC responses, remote-brain responses and brain endothelial aging must be treated as distinct lines of evidence, not as a demonstrated endothelial-to-brain causal chain.

Nicotinamide adenine dinucleotide (NAD+) provides a complementary, experimentally tractable context for cellular transitions. Recent work implicated NAMPT-dependent NAD+ control in endothelial quiescence and stabilization[11]. A distinct REV-ERBα–NFIL3–CD38 axis regulates brain NAD+ in tauopathy[12]. Because these mechanisms were established in the source studies, their inclusion here tests transcriptomic convergence under previously published perturbations; it does not constitute newly performed mechanistic experimentation.

Two design challenges guided the analysis. First, repeated measurements were accepted only when subject linkage was directly recoverable; the public GSE64711 records were not forced into a patient-level longitudinal model. Second, signatures had to be defined before evaluation in the next data context. The frozen age-associated late response was therefore tested in human recovery samples without optimizing gene membership to clinical outcome. This approach allows evidence of non-replication to remain informative, and distinguishes descriptive cross-system compatibility from causal validation. The comparison of signed ageing-state components was emphasized because direction-dependent ortholog loss could otherwise distort a single composite score.

We therefore organized public human and mouse datasets around prespecified evidence roles. A longitudinal human reference defined stress, maintenance and repair programmes; age-stratified mouse polytrauma tested late-response remodeling; human cohorts evaluated recovery associations and cross-species portability. Independent endothelial and brain datasets provided circulatory and neurovascular context, while frozen-reference reanalysis of NAD+ perturbations tested the state-transition framework. We hypothesized that aging would be associated with selective failure to resolve late injury-related states rather than uniformly heightened inflammation, and that NAD+-sensitive endothelial remodeling could offer mechanistic context without proving mediation of trauma recovery.

2. Methods

2.1 Study design, data sources and replication

We conducted a secondary analysis of publicly available longitudinal trauma, mouse aging, clinical recovery, endothelial and NAD+-perturbation datasets (Supplementary Table S1). Human datasets comprised GSE36809, GSE295174, GSE295173, Glue Grant 2/Mendeley, and GSE172210; mouse datasets comprised GSE70418, GSE146395, GSE172382 and GSE255975; GSE318549 supplied an independent HUVEC perturbation model. The Rowe et al. targeted rat brain tables provided regional external context. GSE64711 was evaluated but excluded from formal longitudinal inference because patient–sample–time linkage could not be defensibly reconstructed. Datasets were analyzed separately; cross-study comparisons used predefined scores, orthologs, effect direction or pathway results, not pooled expression matrices.

Biological patients, donors, mice and experimental samples served as inferential units when independent replicates were available. Paired/repeated observations were modeled accordingly. Cells and nuclei were not treated as independent animals or donors. The analysis was designed to preserve negative findings and predefined evidence roles across datasets.

2.2 Frozen programmes, preprocessing and projection

Four predefined analysis sets were held fixed across datasets: SP1 stress-remodeling (178 genes), SP2 maintenance/proteostasis (112), published TraumaRepair_Green (216) and TraumaStress_Red (171). NAD-supply, depletion, SIRT-maintenance and endothelial-stability sets were contextual; the 311-gene aged-late signature, 6,507-gene endothelial transition core and 2,518-gene PS19 disease core were frozen within their specified discovery contrasts before subsequent testing (Supplementary Table S2). Dataset-specific normalizations followed assay design: TMM-logCPM for bulk counts, limma for appropriate processed microarray/log-transformed matrices and Seurat workflows for single-cell/nucleus data.

Programme scores were means of measurable fixed-set genes, with directions frozen where signed scores were needed. Projection of sample x onto a reference contrast $v = \text{mean}(B) - \text{mean}(A)$ used $[(x - \text{mean}(A)) \cdot v]/[v \cdot v]$, anchoring the two reference centroids at 0 and 1; values are transcriptomic coordinates rather than percentages of functional recovery. Mouse–human translation required unambiguous one-to-one orthologs identified without inspecting recovery outcomes. Gene symbols were mapped and duplicated probes collapsed under the frozen primary rule, with alternatives assessed in sensitivity analyses.

2.3 Human trauma trajectories and clinical recovery

Repeated-subject whole-blood profiles in GSE36809 were analyzed using subject-intercept mixed models: programme score ~ nominal time + centered age + sex + (1 | subject). Technical duplicates were collapsed; healthy controls were external comparators. Likelihood-ratio tests assessed omnibus time effects, with balanced 113-subject four-window, exact-time spline and within-patient paired sensitivity analyses. The original longitudinal trauma cohort has been described previously[13].

In GSE295174, CD14+ monocyte counts were aggregated to donor level (fast recovery [FR], n = 8; slow recovery [SR], n = 8; healthy controls, n = 4); technical batches were not counted as donors. The predefined repair–stress balance was TraumaRepair_Green − TraumaStress_Red. Four GSE295173 matched day-3/day-7 donors provided unstratified paired changes. Clinical associations in linked GSE36809/Glue Grant 2 records used age/sex-adjusted

landmark Cox models and Fine–Gray competing-risk sensitivity analyses, with follow-up beginning at the actual sampling time. Recovery definitions and the single-cell source cohort were reported previously[2].

2.4 Aging-by-polytrauma and cross-species transfer

GSE70418 included 36 terminal mouse circulating-leukocyte samples across young (6–10 weeks) and aged (20–24 months) mice at naive, 2-h, day-1 and day-3 states (young n = 4/4/6/4; aged n = 4/5/4/5). Prespecified Age × State contrasts, difference-in-differences and omnibus interaction tests used gene-level and fixed-score limma models. A day-3 high-confidence interaction threshold (BH-FDR < 0.05 and |log fold change| ≥ 0.5) yielded the 311-gene aged-late signature (188 old-excess, 123 old-deficit), frozen before human comparisons. Distance from age-matched naive states, marker-proxy composition adjustment, alternative probe collapse and leave-one-sample-out analyses assessed robustness. The source aging/polytrauma model was reported previously[14].

Strict one-to-one ortholog mapping produced 212 human orthologs; platform coverage and near-zero variance filtering were recorded separately. Old-excess and old-deficit components were evaluated independently in FR/SR and landmark outcome models because their ortholog retention was asymmetric.

2.5 Trauma-derived vesicles and remote-brain transcription

In GSE172210, HUVECs were exposed to plasma small extracellular vesicles from six healthy controls and six trauma donors, each supplying paired 4-h (PT4) and 24-h (PT24) samples. Log2(FPKM + 1) values were analyzed by donor-aware limma with duplicateCorrelation; contrasts were PT4 versus healthy controls, PT24 versus healthy controls and PT24 versus PT4. Persistence was assessed using whole-gene signed-effect concordance and prespecified Hallmark enrichment, with leave-one-trauma-donor-out and fixed-donor sensitivities. The experimental transfer paradigm was published previously[5].

Rowe et al. targeted RT-qPCR data for non-blast burn and complex-extremity injury were used as independent remote-brain context across eight regions and 6, 24 and 168 h, not as genome-wide validation[6]. Rat–human mapping was restricted to strict orthologs; comparisons summarized region-time effect direction and leading-edge genes present in the targeted assay. A missing evaluable endothelial counterpart was not automatically counted as directional discordance (Supplementary Tables S6–S7).

2.6 Brain endothelial aging and circulating plasma

GSE146395 single-cell data were processed with Seurat v5 and canonical correlation analysis to assign arterial, capillary and venous endothelial states, using marker panels and experiment stratification. Frozen natural-aging gene directions were defined in 2,034 cells (981 young and 1,053 aged), including a 406-gene capillary-aging signature, before aged- or young-plasma responses were evaluated. Pooled, balanced, capillary-core and high-confidence sensitivity analyses assessed signed shifts in aging-related redox and barrier/transport genes. Original experiments established age-sensitive brain endothelial responses to plasma; computational single-cell integration followed established methods[15, 16].

GSE172382 served as a separate cortical endothelial-nucleus context (579 endothelial nuclei after QC; young 374, old 205). Its original study investigated NAD+-related blood–brain barrier aging[17]. Because animals were pooled into one sequencing sample per age group, equal-cell downsampling intervals were treated as descriptive sensitivity ranges rather than biological-replicate confidence intervals (Supplementary Table S8).

2.7 NAD+ blockade–rescue and orthogonal mouse disease model

GSE318549 comprised five HUVEC groups (CTL-D2, CTL-D5, FK-D2, FK-D5, FK+NMN-D5; n = 3 each) from a published NAMPT inhibition/NMN rescue experiment[11]. The untreated CTL-D2-to-CTL-D5 contrast defined a 6,507-gene transition core before treatment analysis. Whole-transcriptome, frozen-core and equal-weight signed metrics quantified projection completion; effect-vector correlations and a combined direction/distance criterion measured gene-level restoration. Genome-wide moderated statistics supported Hallmark enrichment. A strict pathway triad required an eligible untreated transition (FDR < 0.05, $|NES| \geq 1.3$), opposite-direction FK866 enrichment and same-direction NMN enrichment, both significant.

GSE255975 hippocampal RNA-seq data (WT 5, RKO 4, PS19 5 and PS19/RKO 6) were reconstructed from raw integer counts and analyzed with edgeR TMM, voomWithQualityWeights and robust limma empirical Bayes. PS19 versus WT fixed a 2,518-gene disease core before assessing RKO. Prespecified tests evaluated PS19/RKO directional reversal, Nfil3, Cd38 and Nampt, and the 21 Hallmark pathways frozen in HUVECs. Only pathways satisfying both disease and counter-directional RKO significance qualified as strict cross-context convergence. The source mouse study investigated REV-ERBα–NFIL3–CD38 regulation of NAD+ in tauopathy[12].

2.8 Statistics, sensitivity analyses and ethics

Tests were two-sided unless direction was fixed prospectively. BH false-discovery rates were controlled by gene or prespecified programme/pathway family; effect sizes and available uncertainty estimates accompanied q values. Additional analyses included exact-time and paired designs, cell-composition adjustment, donor exclusion, ortholog restriction, probe-collapse variation, matched-cell resampling and exclusion of one low-weight mouse RNA-seq sample; full specifications are in Supplementary Methods and Tables S1–S12. R analyses used limma, edgeR, lme4/lmerTest, emmeans, Seurat, fgsea, msigdbr and standard annotation packages. This project generated no new human or animal samples and reanalyzed publicly shared, de-identified data under the originating studies' approvals. Derived gene lists, plotting source data and reproducible code will be made available through the repository specified in the Data Availability Statement before submission.

3. Results

3.1 Longitudinal human trauma programmes show distinct trajectories

GSE36809 supported subject-linked longitudinal analysis; four fixed programmes (SP1, SP2, TraumaRepair_Green and TraumaStress_Red) were scored without downstream reselection. In the balanced 113-patient, four-window subset (452 repeated observations), omnibus time tests were significant for SP1 ($\chi^2 = 91.054$, BH $q = 5.20 \times 10^{-19}$), SP2 ($\chi^2 = 67.810$, $q = 4.02 \times 10^{-14}$), Green ($\chi^2 = 12.019$, $q = 0.00976$) and Red ($\chi^2 = 106.993$, $q = 2.60 \times 10^{-22}$). Exact-time and paired analyses retained the temporal patterns (Supplementary Fig. S1; Supplementary Tables S1–S3).

3.2 Aging changes acute programmes and the late leukocyte transcriptome

We analyzed 36 young and aged mouse samples after polytrauma (Fig. 1A). Age × State interactions were significant for SP1, SP2, Green and Red (BH $q = 0.0071$, 5.2×10^{-4}, 0.0019 and 0.0098, respectively). Day-1 old–young difference-in-differences effects ranged from 0.281 to 0.486 (all $q \leq 0.024$); none of the four predefined programmes retained a significant day-3 difference-in-differences after correction (all $q \geq 0.072$; Fig. 1B; Supplementary Fig. S2; Table S4).

Whole-transcriptome distance from the age-matched naive centroid was greater in aged mice at day 3 (old–young difference = 1.219, BH $q = 0.0012$), with a significant day-3 versus 2-h interaction (estimate = 0.740, $q = 0.0091$; Fig. 1C). Among genes with FDR < 0.05 and $|\log FC| \geq 0.5$ in age-by-trauma interaction contrasts, 7 were detected at 2 h, 289 at day 1 and 311 at day 3. The 311-gene day-3 signature included 188 old-excess and 123 old-deficit genes; 310 were late-exclusive by the prespecified criterion (Fig. 1D; Supplementary Table S4). Day-1 and day-3 gene-level interaction effects were weakly anticorrelated (Pearson $r = -0.052$; Spearman $\rho = -0.111$; Fig. 1E).

Only one signature member, Fcer1a, belonged to a prespecified lineage-marker set. Composition-proxy adjustment retained the direction of all 311 effects (Pearson $r = 0.891$) but reduced median absolute magnitude to 48.5%; adjusted day-3 transcriptome distance remained elevated in aged mice ($\beta = 0.957$, $P = 0.0067$). Alternative probe summarization yielded Pearson $r = 0.976$ and complete directional concordance with primary day-3 interaction effects (Fig. 1F; Supplementary Fig. S2; Supplementary Tables S4 and S12).

3.3 A repair–stress score tracks human recovery trajectories

At day 3 in GSE295174, donor-level CD14+ monocytes from eight fast-recovery (FR), eight slow-recovery (SR) and four healthy-control donors were scored with fixed programmes. Relative to FR, SR showed lower SP1 (−0.446), SP2 (−0.544) and Green (−0.504), with little Red difference (+0.035); none of these four individual comparisons passed BH correction (minimum $q = 0.101$). The prespecified Green-minus-Red score (ΔGvsR) was lower in SR (SR−FR = −0.539, $P = 0.00769$), with unchanged direction across 16 leave-one-donor-out fits (Fig. 2A,B; Supplementary Fig. S3; Table S5).

In four paired GSE295173 donors, ΔGvsR increased between days 3 and 7 (mean change +1.538; paired t-test $P = 2.65 \times 10^{-4}$; exact two-sided sign-flip $P = 0.125$; Fig. 2C). In linked GSE36809/Glue Grant outcome data, ΔGvsR was not associated with later recovery at the earliest 12-h landmark (HR 1.06; $P = 0.476$). Higher ΔGvsR was associated with faster subsequent recovery at days 1, 4, 7 and 14 (HR 1.39, 1.28, 1.55 and 1.70; corresponding BH $q = 0.0086$, 0.0259, 0.0086 and 0.019; Fig. 2D). The day-1 proportional-hazards assumption was violated ($P = 2.87 \times 10^{-4}$); in a time-varying model the association was concentrated in the first subsequent 7 days (HR 1.57, 95% CI

1.22–2.04). Competing-risk and death-exclusion sensitivity estimates retained the association direction (Fig. 2E,F; Supplementary Table S5).

3.4 Aged-late genes show selective links to subsequent human recovery

Strict orthology retained 212 human homologues of the 311 mouse day-3 genes; 211 were scoreable for Figure 3. Retention was lower for old-excess than old-deficit genes (110/188 versus 101/123; Fisher odds ratio 0.29, $P = 6.1 \times 10^{-6}$). After near-zero-variance exclusion, 200 genes were analyzed in GSE295174 (100 per component; Fig. 3A). Neither old-excess nor old-deficit separated SR from FR at day 3 after adjustment (SR−FR effects −0.237, BH q = 0.212; and −0.158, q = 0.414; Fig. 3B,C; Supplementary Fig. S3; Table S5).

In the outcome-linked GSE36809/Glue Grant cohort, the day-7 old-excess score was associated with slower subsequent recovery (HR per SD 0.605, 95% CI 0.469–0.780; BH q = 0.0010). The day-7 old-deficit association (HR 0.654; q = 0.0625) and signed balance (HR 0.772; q = 0.217) did not survive multiplicity correction. The old-excess association persisted with high-support orthologs (HR 0.605), a late-exclusive definition (HR 0.604) and competing-risk modeling (subHR 0.613, 95% CI 0.493–0.763; Fig. 3D,E; Supplementary Table S5).

3.5 Trauma signals show persistent endothelial and time-dependent remote-brain overlap

In GSE172210, HUVECs were exposed to vesicles from six healthy controls and six trauma donors sampled at 4 h (PT4) and 24 h (PT24), with paired trauma-donor exposures (Fig. 4A). Among 13,927 expressed genes, PT4 versus control yielded one FDR-significant gene, PT24 versus control four, and PT24 versus PT4 none. The signed PT4- and PT24-control contrasts correlated across genes (Pearson r = 0.765; Spearman ρ = 0.750; 78.6% same direction). Six leave-one-trauma-donor-out analyses retained the overall direction. Sixteen of 17 prespecified Hallmark pathways persisted across time points; positive signals included TNFA/NF-κB, IL6–STAT3, inflammatory response and hypoxia, whereas cholesterol homeostasis was reduced (Fig. 4A,C; Supplementary Fig. S4A–D; Table S6). Targeted Rowe et al. RT-qPCR tables showed 78/90/65 significant gene–region responses after burn injury (BU) and 105/53/57 after complex-extremity injury (CEI) at 6/24/168 h, respectively; 28 responses met 24-to-168-h persistence criteria (BU 23; CEI 5; Supplementary Fig. S4E; Table S7). Strict orthology identified 66/74 Rowe genes, of which 26 occurred in the filtered HUVEC data. Median directional alignment at 6/24/168 h was 0.116/0.514/−0.002 after BU and 0.136/0.666/−0.080 after CEI, peaking at 24 h (Fig. 4B). At the pathway level, concordant significant brain-event fractions were 46/48 for TNFA/NF-κB, 13/13 for IL6–STAT3, 22/24 for inflammatory response and 30/30 for hypoxia (Fig. 4C). VEGFA, NFKB1, PTGS2, IL6, TGFB1 and VCAM1 were concordant in the shared core; CEBPD and IL12A were discordant examples (Fig. 4D). In the reported aggregate, 103 of 182 significant mapped events were concordant (56.6%); the remaining 79 were not subdivided further because event-level evaluability requires source-table verification (Fig. 4D,E; Supplementary Tables S6–S7).

3.6 Brain endothelial aging shows selective redox and transport changes

GSE146395 yielded 2,034 reconstructed brain endothelial cells (981 young, 1,053 aged): 441 arterial, 1,310 capillary and 283 venous cells (Fig. 5A). Across four experiments, capillary aged–young gene-z-score differences were +0.083 for Txnrd1, +0.101 for Sod2, +0.111 for Abcb1a, −0.140 for Slco1a4, −0.096 for Mfsd2a and −0.088 for Ocln (Fig. 5B; Supplementary Fig. S5; Table S8).

Against a frozen 406-gene natural-aging direction, aged plasma produced small signed-score shifts (pooled +0.0064; capillary-core +0.0339), whereas young plasma yielded consistently negative shifts (pooled −0.0942; balanced −0.0807; capillary-core −0.0993; Fig. 5C,D). Expected-direction fractions ranged from 53.2% to 56.7% for aged-plasma recapitulation and 58.4% to 59.9% for young-plasma reversal. In GSE172382, equal-cell comparisons of 579 reconstructed endothelial nuclei (374 young, 205 aged) showed decreases in Ptprb (−0.474), Tjp1 (−0.298) and Cldn5 (−0.223), with an increase in Ocln (+0.173; Fig. 5E; Supplementary Fig. S5; Supplementary Tables S8 and S12). Resampling ranges reflect pooled-sample sensitivity rather than biological-replicate uncertainty.

3.7 Published NAD+ perturbation models support endothelial transition sensitivity

In GSE318549, the untreated HUVEC day-2-to-day-5 contrast defined a 6,507-gene transition core (3,239 D5-up, 3,268 D5-down). Exclusion of the most heterogeneous untreated D5 sample retained Pearson r = 0.974, Spearman ρ = 0.968 and 100% effect-direction agreement (Fig. 6A; Supplementary Fig. S6A,B; Table S9). Whole-transcriptome, frozen-core and equal-weight signed projections positioned FK866-treated D5 cells at 0.538, 0.536 and 0.528 on the untreated 0-to-1 transition axis; NMN-supplemented D5 cells reached 1.071, 1.061 and 1.054 (Fig. 6B). No genes reached FDR < 0.05 for FK-D2 versus CTL-D2, compared with 3,913 for FK-D5 versus CTL-D5 and 81 for FK+NMN-D5 versus CTL-D5 (Supplementary Fig. S6C; Table S9). Within the frozen core, FK866 direction opposed normal transition (Spearman ρ = −0.895; 93.7% opposite direction), whereas NMN aligned with it (ρ = 0.890; 90.3% same direction). A strict direction-plus-distance criterion was satisfied by 4,376/6,507 genes (67.3%; Fig. 6C; Supplementary Fig. S6E). Of 31 significant untreated-transition Hallmark programmes, 21 met the prespecified FK866-opposition/NMN-restoration triad (Fig. 6D; Supplementary Fig. S6D; Table S10).

In the independent GSE255975 hippocampal PS19/RKO model, 2,301 of 2,518 disease-core genes (91.4%) shifted opposite the PS19–WT direction. PS19/RKO projections on the WT-to-PS19 axis were 0.613 genome-wide and 0.645 within the disease core. Relative to PS19, Nfil3 increased (log2FC +1.114, FDR = 0.0027), Cd38 decreased (−0.927, FDR = 0.013) and Nampt was unchanged after FDR correction (Fig. 6E; Supplementary Fig. S7; Table S11). Only oxidative phosphorylation among the 21 frozen HUVEC triad pathways met the strict PS19/RKO cross-context criterion (NES −1.85 for PS19 versus WT; +1.85 for PS19/RKO versus PS19; Fig. 6F; Supplementary Fig. S7; Tables S11–S12).

4. Discussion

This integrative analysis suggests that aging modifies the temporal organization of post-traumatic immune remodeling rather than simply amplifying early inflammatory responses. In mice, age-by-injury interactions across four predefined stress, maintenance and repair programmes were most prominent at day 1, whereas aged animals remained farther from their age-matched naive transcriptomic state at day 3. This dissociation indicates that convergence of broad programme scores need not imply convergence of the underlying gene-expression state. Aging affects interconnected processes of proteostasis, metabolism and immune communication[3]. The concept of immune resilience likewise distinguishes coordinated adaptation to inflammatory stress from chronological age or isolated inflammatory measurements[18]. Nevertheless, transcriptomic distance is not itself a validated measure of functional recovery.

The frozen 311-gene aged-late signature further separated the late response into old-excess and old-deficit components, arguing against a uniformly hyperinflammatory interpretation. Persistence of the principal effect directions after leukocyte-composition adjustment and alternative probe summarization reduces the likelihood that the signal arises solely from measured cell-mixture or probe-processing artifacts. The attenuation of effect sizes after adjustment nevertheless indicates that cellular composition may contribute to the observed phenotype. Aging-related immune dysfunction involves interactions among immune cells, tissue environments and senescence-associated inflammatory signals[19]. DNA-damage-linked inflammation provides another established context for age-dependent responses, although it was not directly tested here[20]. Importantly, different mice contributed samples at successive time points, so the observed day-3 deviation describes group-level states rather than delayed recovery trajectories within individual animals. Earlier age-stratified trauma experiments similarly identified substantial alterations in post-injury immunity in older mice[14].

The human recovery analyses highlight the potential value of coordinated immune programmes rather than isolated markers. At day 3, individual programme scores did not significantly distinguish fast from slow recovery after multiplicity correction, whereas the prespecified Green-minus-Red repair–stress balance differed between groups. Its association with subsequent recovery also depended on the sampling landmark, with no clear signal at 12 hours and stronger associations at several later time points. Independent clinical research has shown that recovery from acute inflammation can be characterized by coordinated trajectories of circulating leukocyte and platelet counts rather than a single static measurement[21]. Trauma single-cell research has also linked subacute monocyte-network remodeling with faster recovery, providing a more directly relevant transcriptomic comparison[2]. However, subtracting two expression scores does not establish antagonism between biological repair and stress, and the four paired day-3/day-7 donors provide limited inferential support despite concordant directions (exact two-sided sign-flip $P = 0.125$). A violated proportional-hazards assumption at the day-1 landmark further supports time-dependent rather than constant-effect interpretation.

Cross-species transfer provided a separate test of whether the aged mouse late-state signature carried information about human outcomes. Neither the old-excess nor old-deficit component significantly separated day-3 human recovery groups after adjustment, but the day-7 old-excess component was associated with slower subsequent recovery in landmark and competing-risk analyses. This contrast is consistent with temporally selective associations rather than universal replication of an aged transcriptional state. Differences in sample size, assay, leukocyte composition and clinical timing could also account for the day-3 null result, so it cannot establish the absence of a biologically relevant early signal. Unequal strict-ortholog retention between old-excess and old-deficit genes adds

another constraint on score comparisons. Multi-modal measures of human immune health can reflect aspects of adaptation that are not captured by conventional inflammatory biomarkers[22]. Whether the present scores offer independent prognostic value beyond injury severity, infection, age and existing clinical measures requires external prospective testing.

The repair–stress balance and aged-late signature should therefore be regarded as complementary but noninterchangeable constructs. The first summarizes the relative expression of two previously defined trauma programmes; the second projects an age-by-injury gene signature defined in mouse leukocytes before examination of human outcomes. Their different definitions and distinct sampling windows are scientifically informative, but they do not constitute mutual mechanistic validation. The linked GSE36809 and Glue Grant outcome records also should not be counted as two biologically independent patient cohorts. This distinction separates a reproducible analysis strategy from definitive validation of a clinical biomarker.

The circulation-to-endothelium analyses add a second tissue context for injury-associated transcriptional remodeling. Exposure of HUVECs to trauma-derived small extracellular vesicles produced sparse gene-wise false-discovery significance, yet signed genome-wide responses and several inflammatory Hallmark programmes remained aligned for vesicles collected at 4 and 24 hours. Such a pattern can arise when relatively modest, coordinated effects are distributed across multiple pathway members. Prior experimental work established the capacity of trauma-associated vesicles to propagate inflammatory signaling to recipient endothelial cells[5]. Separately, targeted measurements after extracranial injury documented regional and temporal inflammatory transcriptional responses in rat brain[6]. The strongest observed directional overlap occurred around 24 hours, but the overlap involved a limited set of measurable genes and did not establish that circulating vesicles caused the remote-brain responses. Nor do exposures to two vesicle preparations demonstrate that the same endothelial cells remained transcriptionally altered over time.

Brain endothelial aging provided a distinct opportunity to examine how vascular transcriptional states vary by compartment and circulating milieu. Capillary-enriched profiles showed selected increases in redox-related transcripts alongside heterogeneous changes in transport and junctional genes; neither transcript abundance nor a composite signed score can substitute for a direct permeability assay. Organ- and niche-specific environmental signals are established determinants of endothelial specialization[23]. Human brain vascular atlases additionally demonstrate substantial diversity across endothelial states and anatomical regions[24, 25]. In the present analyses, young-plasma exposure produced a modest shift toward the frozen younger expression direction, whereas aged-plasma exposure showed little consistent recapitulation of natural aging. These incomplete effects should not be described as rejuvenation of measured barrier function. Experimental work in aged mice independently implicates endothelial senescence in blood–brain barrier dysfunction[26, 27]. Other studies identify glycocalyx abnormalities and metabolism-associated endothelial subpopulations as additional, nonidentical features of neurovascular aging[28, 29]. Pooled cortical single-nucleus data remain descriptive because equal-cell resampling does not restore animal-level replication.

The NAD^+ perturbation reanalysis offers a more direct intervention-based test of transcriptomic state-transition sensitivity, although it is independent of the trauma and brain endothelial cohorts. By freezing an untreated HUVEC day-2-to-day-5 transition reference before evaluating intervention, we quantified FK866-associated blockade and NMN-associated restoration along a common molecular axis. Agreement among whole-transcriptome, frozen-core and equal-weight projections, together with strict gene- and pathway-level restoration criteria, indicates a

coordinated transcriptional effect rather than isolated marker changes. The original published experiment established the NAMPT-dependent intervention and its vascular context[11]. Separate experimental work in aged endothelial models showed that NAD^+-linked metabolic alterations can accompany impaired proliferation and that NMN supplementation can improve angiogenic readouts[30]. The current projections must nevertheless remain molecular coordinates: values above the untreated reference do not prove complete functional normalization, and the present reanalysis did not directly measure NAD^+ concentrations or flux.

The independent hippocampal PS19/RKO dataset further constrained generalization of the NAD^+ findings. Although the PS19/RKO expression profile shifted substantially toward a wild-type reference, only oxidative phosphorylation among the 21 HUVEC blockade–rescue pathways met the full strict cross-context criterion. Importantly, oxidative phosphorylation was negatively enriched during the untreated HUVEC day-2-to-day-5 transition; NMN restored that reference direction rather than universally activating oxidative phosphorylation. The published PS19/RKO experiment interrogated a separate REV-ERBα–NFIL3–CD38 axis affecting brain NAD^+ metabolism in tauopathy[12]. Consequently, the restricted shared pathway is compatible with context-dependent metabolic remodeling but does not establish a common upstream NAD^+ mechanism, endothelial-to-brain signaling, or therapeutic efficacy of NMN after trauma.

Taken together, these findings support a testable framework in which the timing and coordination of post-injury transcriptional transitions warrant attention alongside the magnitude of acute inflammation. The age-by-injury evidence comes principally from mouse leukocytes, while the human recovery analyses and independent endothelial/NAD^+ datasets contribute distinct, complementary lines of evidence. This synthesis does not imply a single demonstrated causal pathway linking aging, endothelial remodeling and clinical recovery.

Several limitations warrant consideration. First, this study relied on heterogeneous publicly available datasets that differed in species, tissue sources, experimental designs, and analytical platforms. Although age-dependent responses were examined across multiple post-traumatic time points in mice, different animals were sampled at each time point, preventing direct assessment of within-animal recovery trajectories. Second, the human recovery analyses were observational and potentially affected by injury severity, clinical complications, sampling time, and residual confounding. The paired longitudinal analysis included only four donors, and the GSE36809 and Glue Grant outcome records should not be regarded as independent validation cohorts. Unequal ortholog retention may also have influenced cross-species comparisons. Third, the endothelial experiments used HUVECs rather than brain microvascular endothelial cells, while the remote-brain analyses relied on a targeted rat RT-qPCR panel. Furthermore, pooled cortical single-nucleus samples precluded biological-replicate-level inference. Fourth, the published NAMPT inhibition/NMN rescue and PS19/RKO experiments were conducted in distinct, non-trauma models. Their transcriptomic responses do not establish that NAD^+ availability causally regulates endothelial dysfunction or clinical recovery after trauma. Finally, complete gene-membership files, event-level source tables, figure-level numerical data, and executable analysis code are necessary for independent reproducibility. Future studies should integrate prospective age-stratified trauma cohorts with matched endothelial perturbation experiments and direct measurements of NAD^+ metabolism, redox homeostasis, and barrier function.

In conclusion, aging was associated with a distinct late post-traumatic immune transcriptomic phenotype whose old-excess component showed a selective association with subsequent human recovery. Published NAD^+ perturbation experiments independently demonstrated endothelial state-transition sensitivity, providing a focused rationale for mechanistic experiments rather than proof of a causal route from aging to impaired clinical recovery.

DECLARATIONS

Author Contributions: Conceptualization, C.Z.; methodology, S.G. and C.Z.; formal analysis, S.G.; data curation, S.G., P.Z., J.L., S.C., Z.L. and Y.W.; validation, P.Z., J.L., S.C., Z.L. and Y.W.; visualization, S.G.; writing—original draft preparation, S.G.; writing—review and editing, C.Z., Z.T., P.Z., J.L., S.C., Z.L. and Y.W.; supervision, C.Z. and Z.T.; funding acquisition, Z.T. All authors have read and agreed to the published version of the manuscript.

Funding: This research was funded by the National Natural Science Foundation of China, grant number 81873870 (Z.T.).

Institutional Review Board Statement: Not applicable. This study was a secondary analysis of de-identified, publicly available datasets and involved no new participant recruitment, sample collection, intervention, or animal experimentation. Ethical approval for the original studies was obtained by the investigators of the source cohorts according to their institutional requirements.

Informed Consent Statement: Not applicable to the present secondary analysis. Informed consent was obtained by the investigators of the original human studies as required by their respective protocols.

Data Availability Statement: This study reanalyzed public datasets deposited in the NCBI Gene Expression Omnibus (GEO; https://www.ncbi.nlm.nih.gov/geo/) under GSE64711 (metadata audit only), GSE36809, GSE70418, GSE295174, GSE295173, GSE172210, GSE146395, GSE172382, GSE318549 and GSE255975. Additional outcomes were evaluated using the Glue Grant 2/Mendeley resource; regional brain results were obtained from the published supplementary source tables of Rowe et al. (2024). Dataset roles and inferential restrictions are listed in Supplementary Table S1. No new participant- or animal-level data were generated.

Acknowledgments: The authors thank the investigators and participants of the original studies for generating and sharing the datasets analyzed in this work.

Conflicts of Interest: The authors declare no conflicts of interest. The funder had no role in the design of the study; in the selection, analysis, or interpretation of data; in the writing of the manuscript; or in the decision to publish the results.

Declaration of Generative AI and AI-Assisted Technologies： During the preparation of this manuscript, the authors used ChatGPT (OpenAI) to assist with English-language editing, manuscript organization, and preliminary scientific figure design. The authors subsequently reviewed and revised the AI-assisted content as appropriate and take full responsibility for the accuracy, integrity, and scientific validity of the final manuscript.

References

1. Moore, A.R., et al., *A consensus immune dysregulation framework for sepsis and critical illnesses.* Nat Med, 2025. **31**(12): p. 4084-4096.
2. Chen, T., et al., *Multi-modal single-cell sequencing reveals network transition in circulating monocytes that aligns with faster recovery in patients with trauma and favours a response to M-CSF.* EBioMedicine, 2026. **130**: p. 106368.
3. Lopez-Otin, C., et al., *Hallmarks of aging: An expanding universe.* Cell, 2023. **186**(2): p. 243-278.
4. Bonaroti, J.W., et al., *Transcriptomic and Proteomic Characterization of the Immune Response to Elective Spinal Reconstructive Surgery: Impact of Aging and Comparison with Traumatic Injury Response.* J Am Coll Surg, 2024. **238**(5): p. 924-941.
5. Seibold, T., et al., *Small Extracellular Vesicles Propagate the Inflammatory Response After Trauma.* Adv Sci (Weinh), 2021. **8**(24): p. e2102381.
6. Rowe, C.J., et al., *Systemic inflammation following traumatic injury and its impact on neuroinflammatory gene expression in the rodent brain.* J Neuroinflammation, 2024. **21**(1): p. 211.
7. Yang, A.C., et al., *A human brain vascular atlas reveals diverse mediators of Alzheimer's risk.* Nature, 2022. **603**(7903): p. 885-892.
8. Todorov-Volgyi, K., et al., *Proteomics of mouse brain endothelium uncovers dysregulation of vesicular transport pathways during aging.* Nat Aging, 2024. **4**(4): p. 595-612.
9. Bieri, G., A.B. Schroer, and S.A. Villeda, *Blood-to-brain communication in aging and rejuvenation.* Nat Neurosci, 2023. **26**(3): p. 379-393.
10. Chen, X., et al., *Small extracellular vesicles from young plasma reverse age-related functional declines by improving mitochondrial energy metabolism.* Nat Aging, 2024. **4**(6): p. 814-838.
11. Zhao, W., et al., *NAD-dependent redox control enables endothelial quiescence and vascular stabilization during angiogenesis.* Cell Metab, 2026. **38**(7): p. 1478-1496 e9.
12. Lee, J., et al., *REV-ERBalpha regulates brain NAD(+) levels and tauopathy via an NFIL3-CD38 axis.* Nat Aging, 2025. **5**(10): p. 2070-2085.
13. Xiao, W., et al., *A genomic storm in critically injured humans.* J Exp Med, 2011. **208**(13): p. 2581-90.
14. Nacionales, D.C., et al., *A Detailed Characterization of the Dysfunctional Immunity and Abnormal Myelopoiesis Induced by Severe Shock and Trauma in the Aged.* J Immunol, 2015. **195**(5): p. 2396-407.
15. Chen, M.B., et al., *Brain Endothelial Cells Are Exquisite Sensors of Age-Related Circulatory Cues.* Cell Rep, 2020. **30**(13): p. 4418-4432 e4.
16. Hao, Y., et al., *Dictionary learning for integrative, multimodal and scalable single-cell analysis.* Nat Biotechnol, 2024. **42**(2): p. 293-304.
17. Zhan, R., et al., *NAD(+) rescues aging-induced blood-brain barrier damage via the CX43-PARP1 axis.* Neuron, 2023. **111**(22): p. 3634-3649 e7.
18. Ahuja, S.K., et al., *Immune resilience despite inflammatory stress promotes longevity and favorable health outcomes including resistance to infection.* Nat Commun, 2023. **14**(1): p. 3286.
19. Bracken, O.V., R.P.H. De Maeyer, and A.N. Akbar, *Enhancing immunity during ageing by targeting interactions within the tissue environment.* Nat Rev Drug Discov, 2025. **24**(4): p. 300-315.
20. Zhao, Y., et al., *DNA damage and repair in age-related inflammation.* Nat Rev Immunol, 2023. **23**(2): p. 75-89.
21. Foy, B.H., et al., *Human acute inflammatory recovery is defined by co-regulatory dynamics of white blood cell and platelet populations.* Nat Commun, 2022. **13**(1): p. 4705.
22. Sparks, R., et al., *A unified metric of human immune health.* Nat Med, 2024. **30**(9): p. 2461-2472.
23. Gomez-Salinero, J.M., D. Redmond, and S. Rafii, *Microenvironmental determinants of endothelial cell heterogeneity.* Nat Rev Mol Cell Biol, 2025. **26**(6): p. 476-495.
24. Walchli, T., et al., *Single-cell atlas of the human brain vasculature across development, adulthood and disease.* Nature, 2024. **632**(8025): p. 603-613.
25. Pfau, S.J., et al., *Characteristics of blood-brain barrier heterogeneity between brain regions revealed by profiling vascular and perivascular cells.* Nat Neurosci, 2024. **27**(10): p. 1892-1903.
26. Novo, J.P., et al., *Blood-brain barrier dysfunction in aging is mediated by brain endothelial senescence.* Aging Cell, 2024. **23**(9): p. e14270.
27. Csik, B., et al., *Senescent Endothelial Cells in Cerebral Microcirculation Are Key Drivers of Age-Related Blood-Brain Barrier Disruption, Microvascular Rarefaction, and Neurovascular Coupling Impairment in Mice.* Aging Cell, 2025. **24**(7): p. e70048.
28. Shi, S.M., et al., *Glycocalyx dysregulation impairs blood-brain barrier in ageing and disease.* Nature, 2025. **639**(8056): p. 985-994.
29. Otu-Boakye, S., et al., *Lipid-laden endothelial cells exhibit a transcriptomic signature linked to blood-brain barrier dysfunction, metabolic reprogramming, and increased inflammation in the aging brain.* Geroscience, 2026. **48**(2): p. 1735-1750.

30. Kiesworo, K., et al., *Nicotinamide mononucleotide restores impaired metabolism, endothelial cell proliferation and angiogenesis in old sedentary male mice.* iScience, 2025. **28**(1): p. 111656.

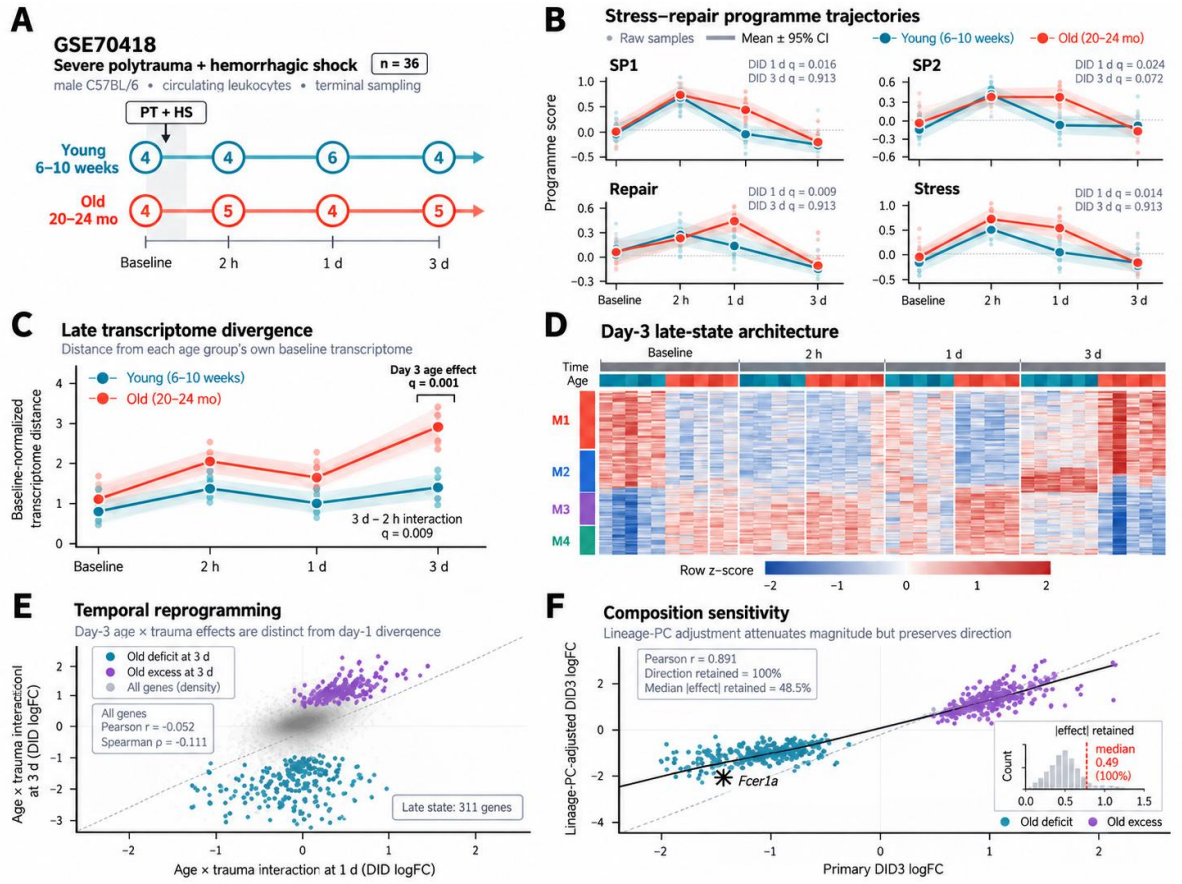


Figure 1 Age-by-polytrauma remodeling of mouse leukocyte trajectories and the late 311-gene state.

(A) GSE70418 design: young (6–10 weeks) and aged (20–24 months) mice at naive, 2 h, day 1 and day 3 (n = 36 independent terminal samples). (B) Frozen SP1, SP2, Green and Red trajectories; points represent animals, lines show group means, and bands show 95% confidence intervals. (C) Distance from age-matched naive transcriptome in 3,000-variable-gene space; day-3 old–young difference = 1.219 (BH q = 0.0012). (D) Heatmap of 311 day-3 Age × State interaction genes (188 old-excess; 123 old-deficit), arranged by sampling group; row clustering is descriptive. (E) Comparison of day-1 and day-3 age-by-trauma gene effects (all-gene Pearson r = −0.052). (F) Primary versus leukocyte-lineage-proxy-adjusted day-3 effects (Pearson r = 0.891); Fcer1a marks the only predefined lineage member. BH adjustment and statistical tests are described in Methods.

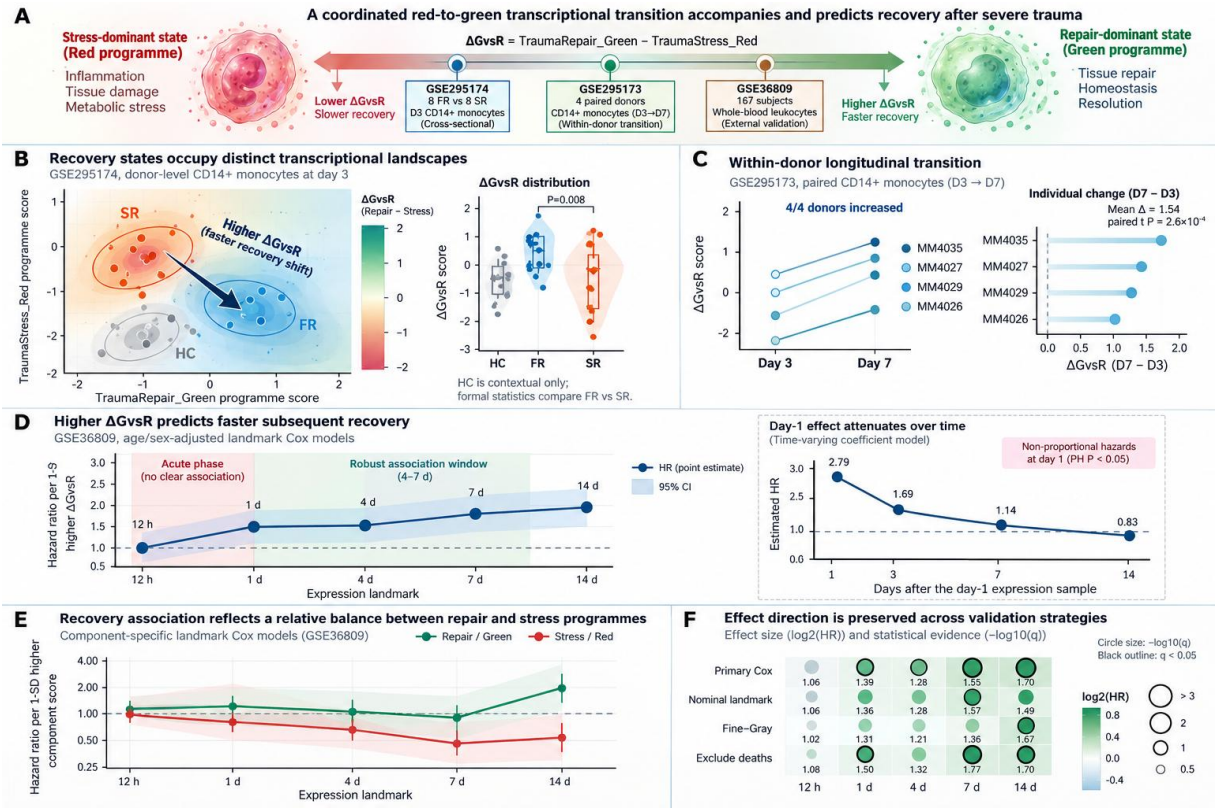


Figure 2. Repair–stress programme balance and subsequent recovery in trauma cohorts.

(A) Study overview of GSE295174 (8 FR, 8 SR), paired GSE295173 (4 donors) and outcome-linked Glue Grant records; ΔGvsR = TraumaRepair_Green − TraumaStress_Red. (B) Day-3 donor-level Green/Red programme landscape and ΔGvsR distributions (healthy controls shown for context). (C) Paired ΔGvsR change from day 3 to day 7 (all four donors increased; mean +1.538; exact sign-flip P = 0.125). (D) Age/sex-adjusted landmark recovery hazard ratios; HR > 1 denotes faster subsequent recovery. Day-1 time-varying effect is shown separately. (E) Component-specific recovery associations for Green and Red programmes.(F) Sensitivity comparison of primary Cox, nominal landmark, Fine–Gray and death-exclusion analyses; statistical significance reflects analysis-specific BH correction.

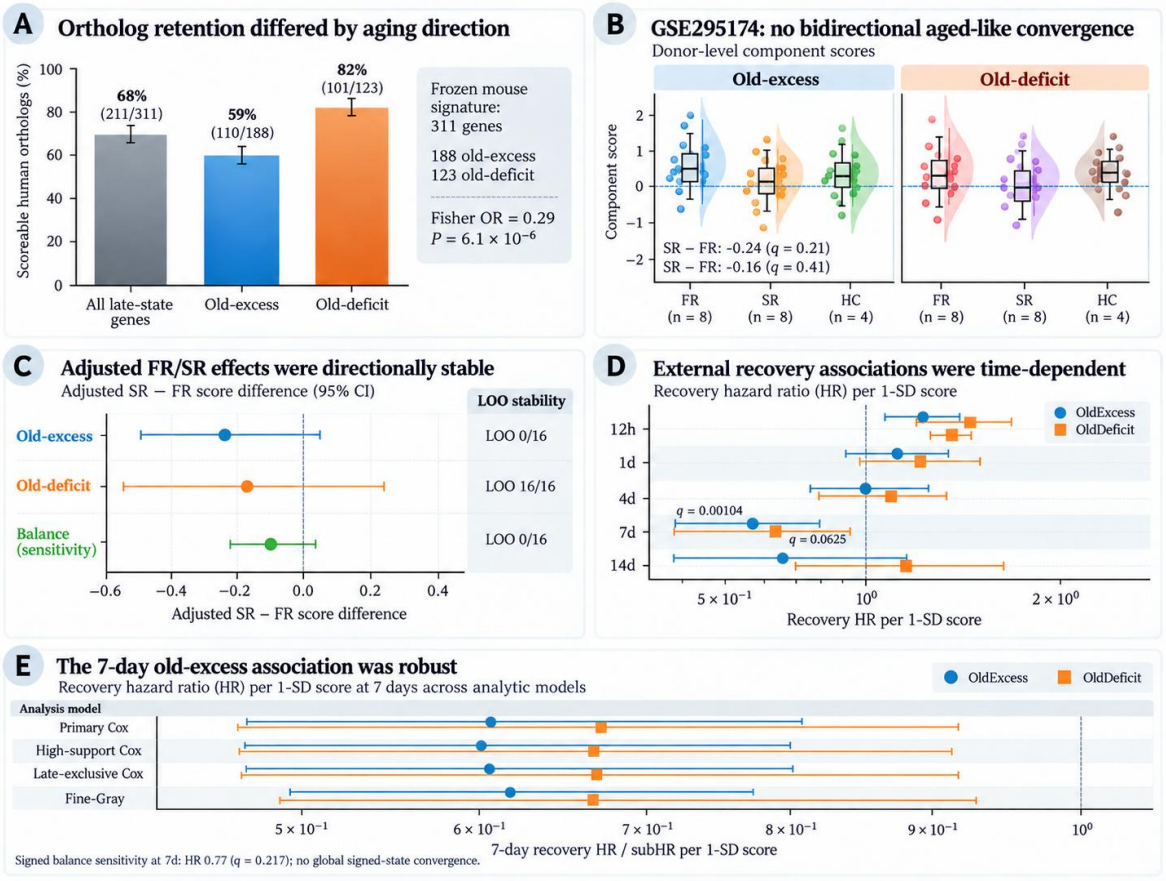


Figure 3. Selective cross-species overlap between mouse aged-late signature and human trauma recovery.

(A) Strict one-to-one ortholog retention from the 311-gene mouse signature; old-excess and old-deficit retention differed ($P = 6.1 \times 10^{-6}$). (B) Mapped component scores in GSE295174 CD14+ monocyte donors (FR n = 8, SR n = 8; HC n = 4 shown descriptively). (C) Adjusted SR−FR old-excess, old-deficit and signed-balance estimates with 95% confidence intervals. (D) Recovery hazard ratios at five clinical landmarks; day-7 old-excess HR = 0.605 (95% CI 0.469–0.780; BH q = 0.0010). (E) Day-7 sensitivity analyses with high-support orthologs, late-exclusive genes and Fine–Gray competing-risk model.

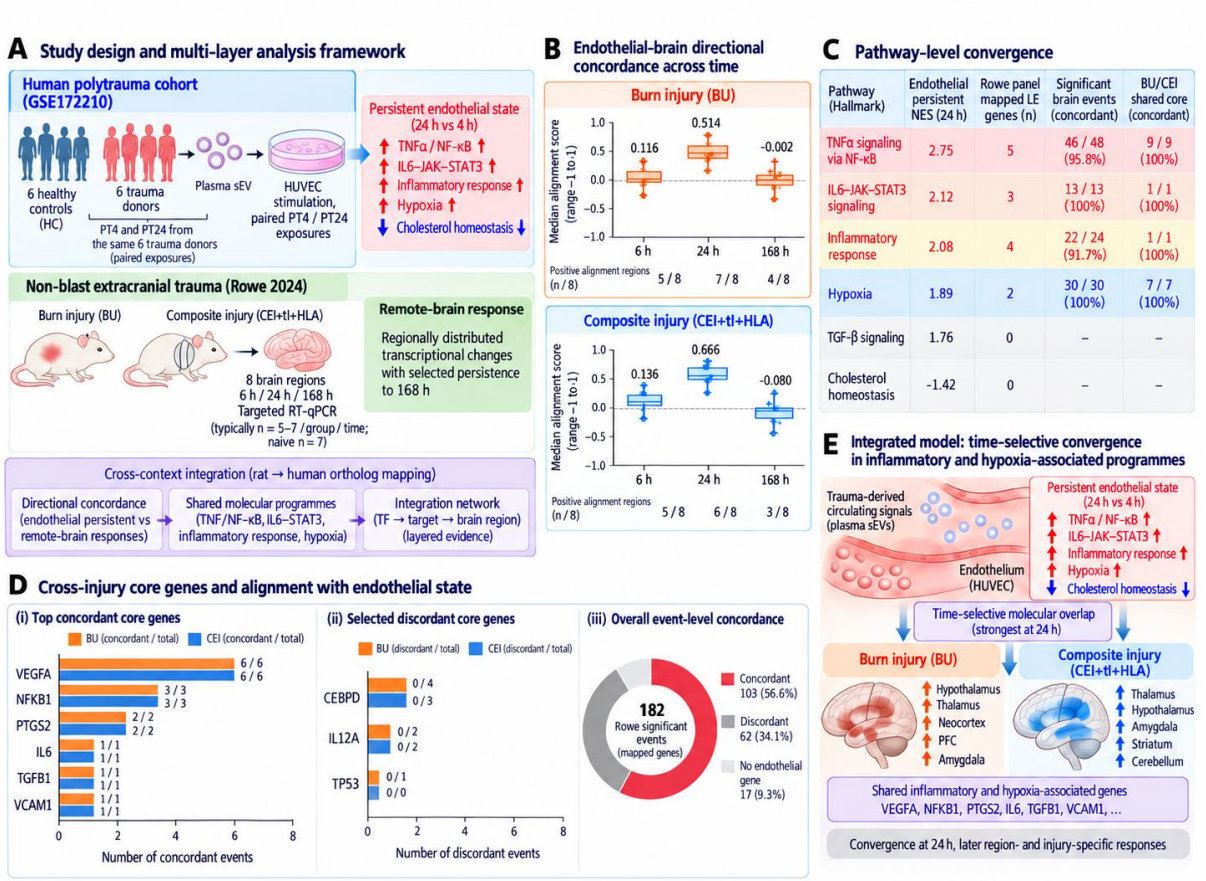


Figure 4. Trauma-sEV endothelial programmes and temporally selective remote-brain molecular concordance.

(A) Paired PT4/PT24 vesicle exposures from six trauma donors versus six controls in HUVECs, alongside independent Rowe targeted rat brain RT-qPCR time-series. (B) Reported median directional endothelial–brain alignment at 6, 24 and 168 h after burn or complex-extremity injury; aggregate values are shown without synthetic sample-level points. (C) Hallmark pathway overlaps for TNFA/NF-κB, IL6–STAT3, inflammatory response and hypoxia; non-measured leading-edge targets were not counted as negative validation. (D) Shared concordant/discordant representative genes and aggregate 103/182 directionally concordant remote-brain events. Subclassification of the other 79 events awaits event-level verification. (E) Conceptual integration of parallel endothelial and regional-brain evidence; cross-context correspondence does not establish endothelial-to-brain causation.

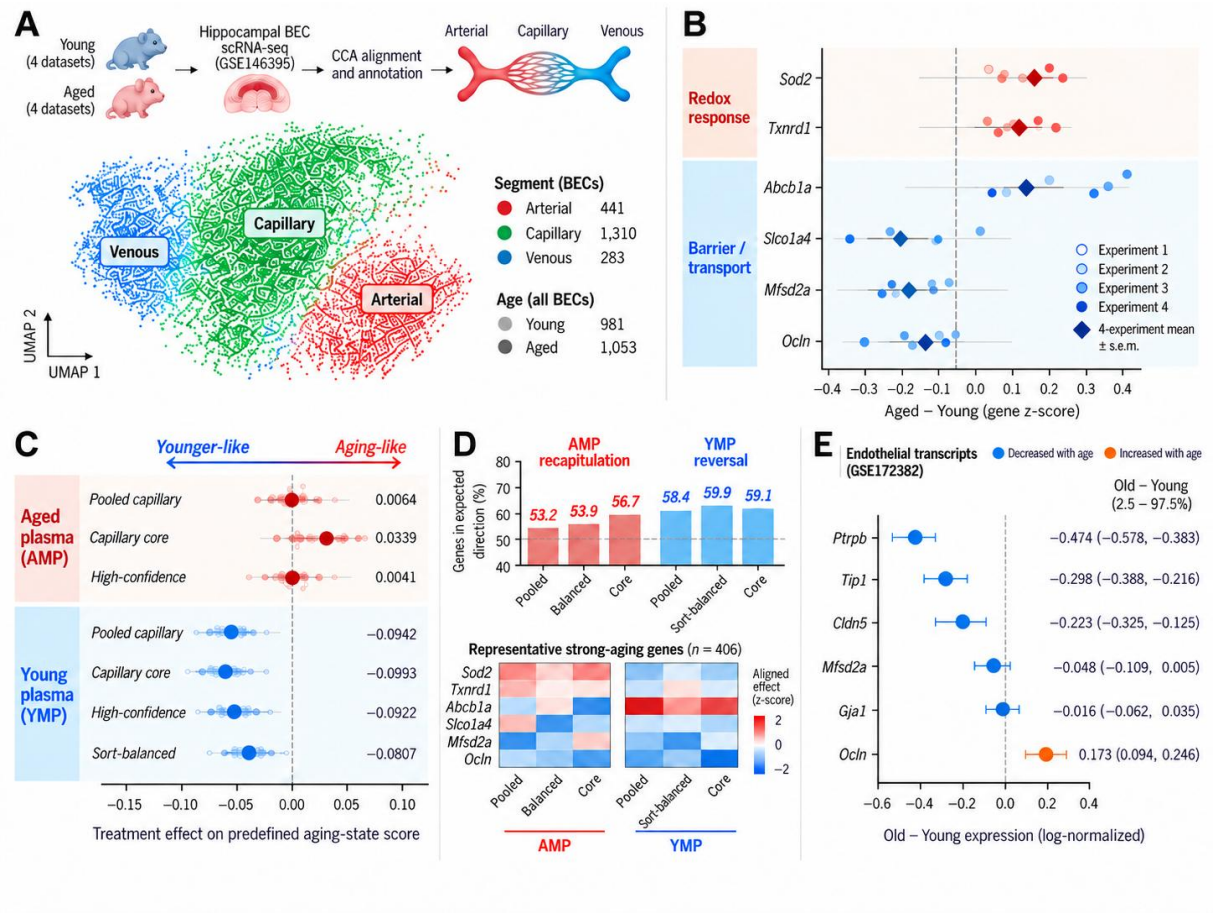


Figure 5. Capillary-enriched endothelial aging and modulation by plasma exposure.

(A) Reconstructed GSE146395 arterial–capillary–venous reference (2,034 brain endothelial cells: 981 young, 1,053 aged). (B) Experiment-stratified aging effects on selected capillary redox and barrier/transport genes; symbols show experimental estimates and group means. (C) Frozen signed capillary aging-state shifts after aged or young plasma in pooled and stratified analyses. (D) Expected-direction concordance of the 406-gene aging set and selected gene effects across analytical variants. (E) Independent GSE172382 cortical endothelial nuclei (young 374, old 205); intervals are 2.5th–97.5th percentiles from equal-cell downsampling, not independent-animal confidence intervals.

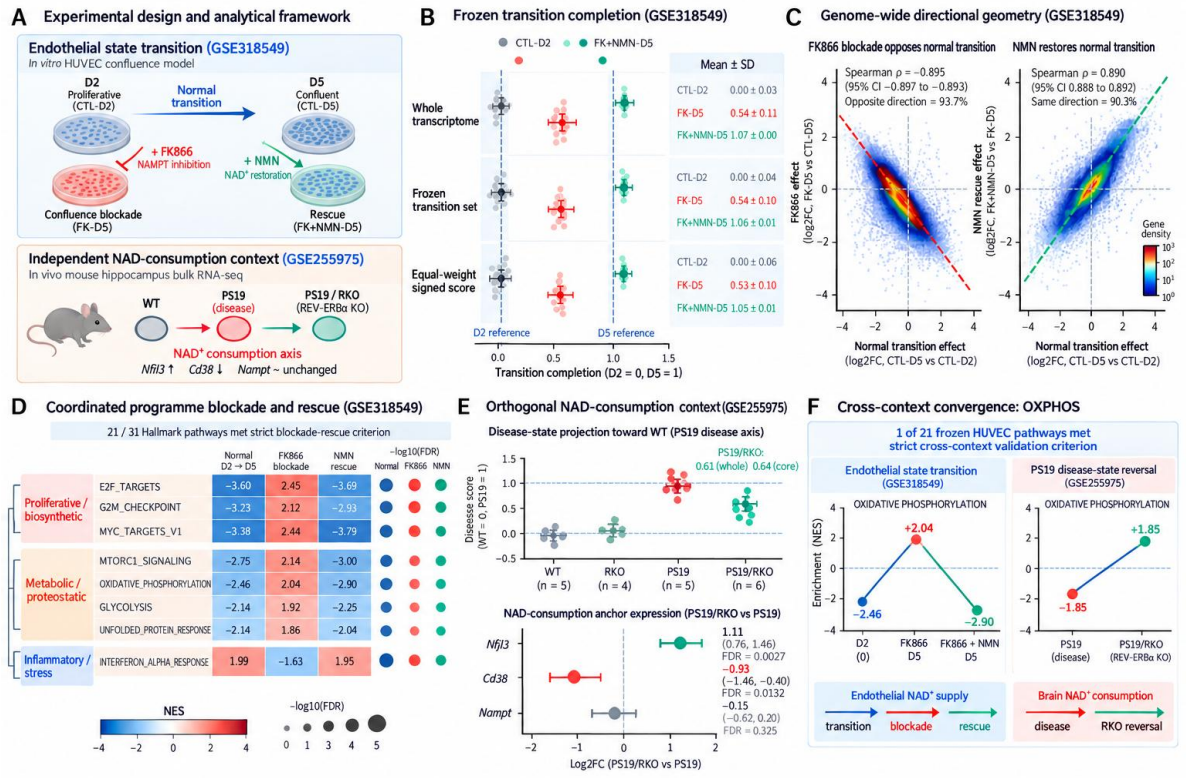


Figure 6. Published endothelial NAMPT blockade–NMN rescue and orthogonal NAD-related pathway context.

(A) HUVEC untreated D2-to-D5 transition defined before FK866/NMN; separate PS19/RKO hippocampal dataset provides orthogonal context. (B) Whole-transcriptome, frozen 6,507-gene and signed-score projections; FK-D5 completion ≈ 0.53 and FK+NMN-D5 ≈ 1.05–1.07 relative to untreated D5 = 1. (C) FK866 opposes (Spearman ρ = −0.895) and NMN aligns with (ρ = +0.890) the frozen transition direction. (D) Representative Hallmark NES from 21 pathways meeting significant blockade–rescue triad criteria. (E) PS19/RKO hippocampal disease-state projection and prespecified Nfil3/Cd38/Nampt gene effects. (F) Oxidative phosphorylation is the sole strict HUVEC-to-PS19/RKO pathway-level convergence; these are different published intervention contexts.

Supplementary Files

This is a list of supplementary files associated with this preprint. Click to download.

- SupplementaryTables.docx
- SupplementaryMaterials.docx